machines

MDPI

Article

Improved Deadbeat Predictive Current Predictive Control Based on Low-Complexity State Feedback Controllers and Online Parameter Identification

Yun Zhang [1,2], Mingchen Luan [1,2,*], Zhenyu Tang [3], Haitao Yan [1,2] and Long Wang [1,2]

[1] School of Rail Transportation, Shandong Jiaotong University, Jinan 250357, China; zhangyun@sdjtu.edu.cn (Y.Z.); 23221027@stu.sdjtu.edu.cn (H.Y.); 23221021@stu.sdjtu.edu.cn (L.W.)
[2] Key Laboratory of Rail Transit Safety Technology and Equipment, Shandong Province Transportation Industry, Jinan 250357, China
[3] Degree Programs in Systems and Information Engineering, University of Tsukuba, 1-1-1 Tennoudai, Tsukuba 305-8573, Ibaraki, Japan; s2465020@u.tsukuba.ac.jp
* Correspondence: 22121003@stu.sdjtu.edu.cn

Abstract

To improve the control accuracy and address the parameter disturbance issues of joint-driven permanent magnet synchronous motors in intelligent manufacturing, this paper proposes an improved deadbeat predictive current predictive control (DPCC) scheme that eliminates dead zones. This scheme establishes a multi-parameter identification model based on the error equation of the *d-q* axis predicted current, which improves the problem of not being able to identify all parameters caused by insufficient input signals. It also implements decoupling compensation for the coupling between the *d-q* axis inductance, stator resistance, and magnetic flux linkage. To meet the anticipated control objectives and account for external disturbances, a low-complexity specified performance tracking controller (LCSPC) based on output target error signals has been designed. This mitigates output delay issues arising from nonlinear components during motor operation. Finally, simulation analysis and experimental testing demonstrate that the proposed control scheme achieves high identification accuracy with minimal delay, thus meeting the transient control performance requirements for motors in intelligent manufacturing processes.

Keywords: deadbeat predictive current predictive control (DPCC); parameter identification; a low-complexity specified performance tracking controller (LCSPC)

check for updates

Received: 28 August 2025
Revised: 25 September 2025
Accepted: 2 October 2025
Published: 5 October 2025

Citation: Zhang, Y.; Luan, M.; Tang, Z.; Yan, H.; Wang, L. Improved Deadbeat Predictive Current Predictive Control Based on Low-Complexity State Feedback Controllers and Online Parameter Identification. *Machines* **2025**, *13*, 917. https://doi.org/10.3390/machines13100917

Copyright: © 2025 by the authors. Licensee MDPI, Basel, Switzerland. This article is an open access article distributed under the terms and conditions of the Creative Commons Attribution (CC BY) license (https://creativecommons.org/licenses/by/4.0/).

1. Introduction

Permanent magnet synchronous motors (PMSMs) offer advantages such as high power density, rapid speed response, and a wide speed regulation range. They are widely used in electric-drive applications, including in smart manufacturing, electric vehicles, robotics, and unmanned aerial vehicles [1,2]. Joint-drive motors, used in the manufacture of equipment, utilize various control strategies, such as proportional–integral (PI) linear control, hysteresis current control, and predictive control, to achieve a superior dynamic response and greater control accuracy [3]. While PI control effectively reduces steady-state error, its fixed switching frequency can result in suboptimal dynamic performance in certain conditions [4]. Hysteresis current control is simple and offers a rapid response; however, current fluctuations during operation may cause peak currents to exceed their limit values [5]. However, predictive control demonstrates favorable dynamic performance in terms of

aspects such as dynamic response and current tracking. Coupled with its straightforward structure and ease of implementation, this makes it a popular choice for permanent magnet synchronous motor control systems [6,7]. Predictive control can be categorized into two main types: Model Predictive Control (MPC) and Discrete-Phase Current Predictive Control (DPCC). MPC algorithms predict the instantaneous current by describing the voltage vector cost function. However, the finite number of voltage vectors inevitably generates current ripple during the prediction process [8]. In contrast, DPCC algorithms that use discrete motor models can obtain a greater number of voltage vectors. This enables the predicted current to track the reference current more accurately [9,10]. However, DPCC is a motor-model-based control method with inherent limitations, as its predictive efficacy depends on the accuracy of the motor model. During motor control, issues arising from parameter mismatch due to parameter variations and model uncertainties can induce significant current harmonics, increased current tracking errors and amplified torque ripple, thereby compromising the stability of the control system [11]. Several improvement methods have been developed to overcome the degradation in control system performance caused by parameter mismatch, such as disturbance estimation [12], compensating controllers [13], and parameter identification [14].

Parameter identification techniques can be divided into two categories: offline parameter identification [15] and online parameter identification [16]. Commonly used online identification methods include extended Kalman filtering [17], recursive least squares [18], and model reference adaptive filtering [19]. Reference [20] proposes a sensorless control parameter identification method that uses current and voltage information to estimate the resistance and back EMF constants under various load conditions. Reference [21] fully considers the impact of stator resistance and magnetic flux uncertainty on the control system and uses MRAS for parameter estimation, but MRAS requires advanced information sampling to enable the identification system to quickly enter the convergence stage. Reference [22] employs a novel adaptive interconnected observer to observe rotor speed, position, and torque and uses a motor model to estimate resistance and inductance. Reference [23] proposes a speed control algorithm that uses system output equations for parameter identification. The robustness of the algorithm is verified when combined with sliding mode control. Reference [24] used a method combining MRAS and Popov superstability theory to derive the discrete-time model for each parameter and fully considered the impact of voltage-type inverters on the identification results. Reference [25] used an identification method based on motor models to estimate resistance and inductance, compared the results with those obtained using EKF identification, and analyzed the advantages and disadvantages of various algorithms. These control strategies mentioned above, based on parameter identification, are very limited in practical applications due to the high complexity of the algorithm. In order to meet more reliable industrial level application algorithms, we designed a low-complexity parameter identification control system.

This paper proposes an enhanced current prediction control strategy without dead time, employing the low-complexity specified performance tracking controller (LCSPC) algorithm, the Dead-Time Control with Current Prediction (DPCC) algorithm, and a parameter decoupling model to achieve closed-loop control. This approach addresses transient model changes in the motor model, enables online identification of electrical parameters, and incorporates state feedback from the control system. The principal contributions of this work are as follows:

(1) Low-complexity state feedback controller. We propose a low-complexity state feedback controller decoupling algorithm based on the predictive error model. This approach acquires parameters without employing nonlinear or adaptive methods within the control

system and does not require the derivative of the expected trajectory. As it involves no hardware computation, it reduces controller costs.

(2) DPCC parameter decoupling. A parameter prediction model and an incremental current error model were derived using a discrete mathematical model of the motor. This approach fully accounts for under-ranking issues during parameter decoupling and provides a compensation reference quantity for the decoupling model.

(3) Online parameter identification control scheme. A DPCC multi-parameter discrete system identification scheme based on LCSPC has been proposed to enhance performance. Using d/q-axis current error as the algorithmic input reduces the dependency of DPCC on motor models while improving the efficiency of state feedback. Consequently, it mitigates the significant d/q-axis current fluctuations caused by parameter mismatch during motor operation.

2. Mathematical Models of Surface-Mounted Permanent Magnet Synchronous Motors

For motor control systems using FOC control strategies, PI algorithms are generally used to control the current loop. For surface-mounted PMSMs, the d-axis reference current is typically set to zero, and the q-axis reference current is determined by the control output of the speed loop. This paper designs an improved parameter identification method for current control without beat frequency based on the motor mathematical model. The voltage equation of the motor in the d-q reference frame can be expressed as (1):

$$\begin{cases} u_d = R_s i_d + L_d \frac{di_d}{dt} - \omega_e L_q i_q \\ u_q = R_s i_q + L_q \frac{di_q}{dt} + \omega_e L_d i_d + \omega_e \psi_f \end{cases} \tag{1}$$

where u_d, u_q, i_d, and i_q are the stator voltage and current in the d-q coordinate system, respectively; R_s is the stator resistance; L_d and L_q are the stator inductances in the *d-q* coordinate system; ω_e is the rotor angular velocity; and ψ_f is the rotor magnetic flux.

The electromagnetic torque equation of the motor can be expressed as (2):

$$T_e = 1.5 p_n \psi_f i_q \tag{2}$$

where T_e is the electromagnetic torque of the motor, and p_n is the number of pole pairs of the motor. The motion equation of the motor can be expressed as (3):

$$T_e = J \frac{d\omega_m}{dt} + B\omega_m + T_L \tag{3}$$

where ω_m is the mechanical angular velocity of the motor, J is the rotational inertia, B is the damping coefficient, and T_L is the load torque.

3. Decoupling of Motor Parameters

3.1. Deadbeat Predictive Current Control Principle

This paper adopts a deadbeat predictive current prediction control algorithm, which has the advantages of a fast dynamic response and small current fluctuations at a constant switching frequency. By detecting the actual current and the given reference current, the voltage value to be applied in the next control cycle is calculated so that the stator current can accurately follow the reference current. The structure of the motor control system is shown in Figure 1.

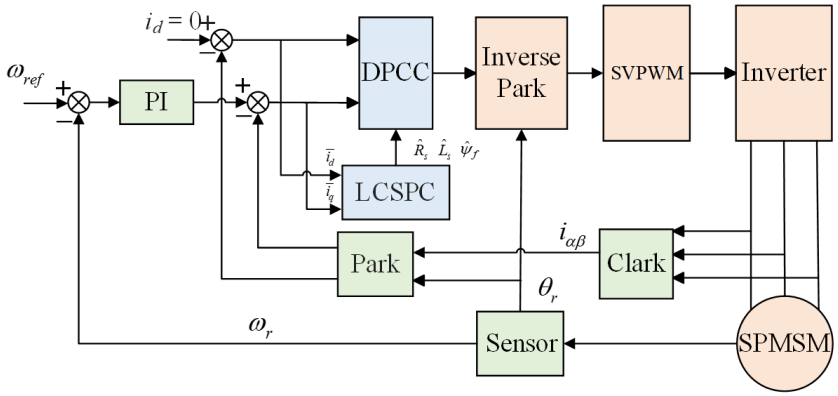

Figure 1. Block diagram of permanent magnet synchronous motor control system structure.

The stator current is discretized using the first-order forward Euler method, as shown in (4):

$$\frac{di_d}{dt} = \frac{i_d(t) - i_d(t-1)}{T_s}, \frac{di_q}{dt} = \frac{i_q(t) - i_q(t-1)}{T_s} \tag{4}$$

where T_s is the sampling period, $i_d(t)$ and $i_q(t)$ represent the sampled currents on the *d*-*q* axis at time *t*, and $i_d(t-1)$ and $i_q(t-1)$ represent the sampled currents on the *d*-*q* axis at time $t+1$.

Substituting (4) into (1), the predicted current value at time $t+1$ can be expressed as (5):

$$\begin{cases} i_d^{pre}(t+1) = (1 - \frac{T_s R_s}{L_d}) i_d(t) + T_s \omega_e(t) i_q(t) \frac{L_q}{L_d} + \frac{T_s}{L_d} u_d(t) \\ i_q^{pre}(t+1) = (1 - \frac{T_s R_s}{L_q}) i_q(t) - T_s \omega_e(t) i_d(t) \frac{L_d}{L_q} + \frac{T_s}{L_q} \left[u_q(t) - \omega_e(t) \psi_f \right] \end{cases} \tag{5}$$

where $i_d^{pre}(t+1)$ and $i_q^{pre}(t+1)$ represent the predicted current values of the *d*-*q* axis at time $t+1$.

According to (5), the expected voltage expression at time $t+1$ is shown in (6):

$$\begin{cases} u_d^{\exp}(t+1) = L_d \frac{i_d(t+2) - i_d^{pre}(t+1)}{T_s} - \omega_e(t+1) L_q i_q^{pre}(t+1) + R_s i_d^{pre}(t+1) \\ u_q^{\exp}(t+1) = L_q \frac{i_q(t+2) - i_q^{pre}(t+1)}{T_s} + \omega_e(t+1) L_d i_d^{pre}(t+1) + R_s i_q^{pre}(t+1) + \omega_e(t+1) \psi_f \end{cases} \tag{6}$$

where $i_d(t+2)$ and $i_q(t+2)$ are the predicted values of the *d*-*q* axis current at time $t+2$, $u_d^{\exp}(t+1)$ and $u_q^{\exp}(t+1)$ are the expected stator output voltages at time $t+1$, and $\omega_e(t+1)$ is the rotor electrical angular velocity at time $t+1$.

Since $i_d(t+2)$, $i_q(t+2)$, and $\omega_e(t+1)$ are unknown at time *t*, the main task of the DPCC model is to ensure that the current sampled at time $t+2$ accurately follows the current sampled at time $t+1$:

$$i_d(t+2) \approx i_d^{ref}(t+1), i_q(t+2) \approx i_q^{ref}(t+1) \tag{7}$$

During the process of reference value changes, assume a time step delay

$$i_d^{ref}(t+1) = i_d^{ref}(t+1), i_q^{ref}(t+1) = i_q^{ref}(t+1), \omega_e(t+1) = \omega_e(t) \tag{8}$$

Substituting (7) and (8) into (6) yields the voltage vector at time $t+1$ as

$$\begin{cases} u_d^{exp}(t+1) = R_s i_d^{pre}(t+1) + L_d \frac{i_d^{ref}(t) - i_d^{pre}(t+1)}{T_s} - \omega_e(t) L_q i_q^{pre}(t+1) \\ u_q^{exp}(t+1) = R_s i_q^{pre}(t+1) + L_q \frac{i_q^{ref}(t) - i_q^{pre}(t+1)}{T_s} + \omega_e(t) L_d i_d^{pre}(t+1) + \omega_e(t) \psi_f \end{cases} \tag{9}$$

In summary, DPCC samples the current and voltage at time t, uses the current reference value at time $t+1$ to calculate the desired voltage at the next moment, and then controls the current value at the next moment to quickly follow the desired value through the PWM signal generated by the SVPWM.

3.2. Inductive Decoupling Based on Current Prediction Error Model

During the operation of permanent magnet synchronous motors, external environments, operating conditions, and other factors can cause deviations in motor electrical parameters, leading to a decrease in DPCC accuracy. This paper approaches the issue from the perspective of motor transient mathematical models, representing the uncertain components of motor parameters in the prediction model. Equation (5) can be expressed as

$$\begin{cases} \tilde{i}_d^{pre}(t+1) = \left[1 - \frac{T_s(R_s+\Delta R_s)}{L_d+\Delta L_d}\right] i_d(t) + T_s\omega_e(t) i_q(t) \frac{L_q+\Delta L_q}{L_d+\Delta L_d} + \frac{T_s u_d(t)}{L_d+\Delta L_d} \\ \tilde{i}_q^{pre}(t+1) = \left[1 - \frac{T_s(R_s+\Delta R_s)}{L_q+\Delta L_q}\right] i_q(t) - T_s\omega_e(t) i_d(t) \frac{L_d+\Delta L_d}{L_q+\Delta L_q} \\ \quad + \frac{T_s}{L_q+\Delta L_q}\left[u_q(t) - (\psi_f + \Delta\psi_f)\omega_e(t)\right] \end{cases} \tag{10}$$

where ΔR_s, ΔL_d, ΔL_q, and Δpsi_f are the uncertainty components of R_s, L_d, L_q, and ψ_f, respectively, and $\tilde{i}_d^{pre}$ and $\tilde{i}_q^{pre}$ are the predicted currents of the d-q axis at time $t+1$.

The actual parameters during the operation of a permanent magnet synchronous motor are expressed as

$$\tilde{R}_s = R_s + \Delta R_s, \tilde{L}_d = L_d + \Delta L_d, \tilde{L}_q = L_q + \Delta L_q, \tilde{\psi}_f = \psi_f + \Delta\psi_f \tag{11}$$

There is coupling between the various parameters of permanent magnet synchronous motors, which affects the performance of motor control. Before performing parameter identification, it is necessary to decouple the relevant parameters in order to eliminate the coupling effects between the parameters to the greatest extent possible.

First, define $\Delta i_d(t+1)$ and $\Delta i_q(t+1)$ as the differences between the actual predicted current and the ideal predicted current, as expressed by the following equations:

$$\begin{cases} \Delta i_d(t+1) = \tilde{i}_d^{pre}(t+1) - i_d^{pre}(t+1) \\ \Delta i_q(t+1) = \tilde{i}_q^{pre}(t+1) - i_q^{pre}(t+1) \end{cases} \tag{12}$$

Substituting (5) and (10) into (12) yields

$$\begin{cases} \Delta i_d(t+1) = T_s i_d(t)\left(\frac{R_s}{L_d} - \frac{R_s+\Delta R_s}{L_d+\Delta L_d}\right) + T_s u_d(t)\left(\frac{1}{L_d+\Delta L_d} - \frac{1}{L_d}\right) + T_s\omega_e(t) i_q(t)\left(\frac{L_q+\Delta L_q}{L_d+\Delta L_d} - \frac{L_q}{L_d}\right) \\ \Delta i_q(t+1) = T_s i_q(t)\left(\frac{R_s}{L_q} - \frac{R_s+\Delta R_s}{L_q+\Delta L_q}\right) + T_s u_q(t)\left(\frac{1}{L_q+\Delta L_q} - \frac{1}{L_q}\right) + T_s\omega_e(t) i_d(t)\left(\frac{L_d}{L_q} - \frac{L_d+\Delta L_d}{L_q+\Delta L_q}\right) \\ +T_s\omega_e(t)\left(\frac{\psi_f}{L_q} - \frac{\psi_f+\Delta\psi_f}{L_q+\Delta L_q}\right) \end{cases} \tag{13}$$

Since the control cycle of the motor is much shorter than the mechanical time constant, it can be assumed that $\omega_e(t)$ remains unchanged between two adjacent cycles. During motor operation, the motor's inductance suppresses changes in current, while the applied voltage can be rapidly adjusted according to changes in the PWM duty cycle. Therefore, it is generally assumed that the rate of change in voltage is much greater than the rate of change in current. The above relationship can be expressed by (14):

$$\begin{cases} \left|\left(\frac{R_s}{L_d} - \frac{R_s+\Delta R_s}{L_d+\Delta L_d}\right)[i_d(t) - i_d(t-1)]\right| \ll \left|\left(\frac{1}{L_d+\Delta L_d} - \frac{1}{L_d}\right)[u_d(t) - u_d(t-1)]\right| \\ \left|\left(\frac{R_s}{L_q} - \frac{R_s+\Delta R_s}{L_q+\Delta L_q}\right)[i_q(t) - i_q(t-1)]\right| \ll \left|\left(\frac{1}{L_q+\Delta L_q} - \frac{1}{L_q}\right)[u_q(t) - u_q(t-1)]\right| \end{cases} \tag{14}$$

Subtracting the prediction errors between two adjacent cycles yields the following equation:

$$\begin{cases} \Delta i_d(t+1) - \Delta i_d(t) = \frac{-\Delta L_d T_s}{(L_d+\Delta L_d)L_d}[u_d(t) - u_d(t-1)] \\ \Delta i_q(t+1) - \Delta i_q(t) = \frac{-\Delta L_q T_s}{(L_q+\Delta L_q)L_q}[u_q(t) - u_q(t-1)] \end{cases} \tag{15}$$

In summary, $\tilde{L}_d$ and $\tilde{L}_q$ can be expressed by (16) as follows:

$$\tilde{L}_d = \frac{T_s L_d}{T_s + L_d \frac{\Delta i_d(t+1) - \Delta i_d(t)}{u_d(t) - u_d(t-1)}}, \tilde{L}_q = \frac{T_s L_q}{T_s + L_q \frac{\Delta i_q(t+1) - \Delta i_q(t)}{u_q(t) - u_q(t-1)}} \tag{16}$$

3.3. Decoupling of Resistance and Magnetic Flux Based on Current Prediction Error Model

The prediction model given by (5) can be used to calculate the prediction increment, as shown in (17):

$$\zeta i_d^{pre}(t+1) = i_d^{pre}(t+1) - i_d^{pre}(t), \zeta i_q^{pre}(t+1) = i_q^{pre}(t+1) - i_q^{pre}(t) \tag{17}$$

The mathematical model of the motor can be used to represent the corresponding current increment model, as shown in (18):

$$\begin{cases} \zeta i_d^{pre}(t+1) = \left(1 - \frac{R_s T_s}{L_d}\right)\zeta i_d(t) + \omega_e(t)\zeta i_q(t) T_s \frac{L_q}{L_d} + \frac{T_s}{L_d}\zeta u_d(t) \\ \zeta i_q^{pre}(t+1) = \left(1 - \frac{R_s T_s}{L_q}\right)\zeta i_q(t) + \omega_e(t)\zeta i_d(t) T_s \frac{L_d}{L_q} + \frac{T_s}{L_q}\zeta u_q(t) \end{cases} \tag{18}$$

where $\zeta i_d(t)$, $\zeta i_q(t)$, $\zeta u_d(t)$, and $\zeta u_q(t)$ are the current and voltage increments in the *d-q* coordinate system, as shown in (19):

$$\begin{cases} \zeta i_d(t) = i_d(t) - i_d(t-1) \\ \zeta i_q(t) = i_q(t) - i_q(t-1) \\ \zeta u_d(t) = u_d(t) - u_d(t-1) \\ \zeta u_q(t) = u_q(t) - u_q(t-1) \end{cases} \tag{19}$$

According to (10), the current increment in the d-q coordinate system can be expressed in terms of the predicted current, and (18) can be rewritten as (20).

$$\begin{cases} \zeta \tilde{i}_d^{pre}(t+1) = \left(1 - \frac{\tilde{R}_s T_s}{\tilde{L}_d}\right)\zeta i_d(t) + \omega_e(t)\zeta i_q(t) T_s \frac{\tilde{L}_q}{\tilde{L}_d} + \frac{T_s}{\tilde{L}_d}\zeta u_d(t) \\ \zeta \tilde{i}_q^{pre}(t+1) = \left(1 - \frac{\tilde{R}_s T_s}{\tilde{L}_q}\right)\zeta i_q(t) + \omega_e(t)\zeta i_d(t) T_s \frac{\tilde{L}_d}{\tilde{L}_q} + \frac{T_s}{\tilde{L}_q}\zeta u_q(t) \end{cases} \tag{20}$$

where $\zeta \tilde{i}_d^{\mathrm{pre}}\left(t+1\right)$ and $\zeta \tilde{i}_q^{\mathrm{pre}}\left(t+1\right)$ are the predicted current increments at time $t+1$ in the *d-q* coordinate system, which is itself a function containing the actual motor parameters.

Subtracting (18) from (20) yields the current prediction error model (21):

$$\begin{aligned} \zeta \tilde{i}_d^{pre}(t+1) - \zeta i_d^{pre}(t+1) = {} & T_s \zeta i_d(t)\left(\frac{R_s}{L_d} - \frac{\tilde{R}_s}{\tilde{L}_d}\right) + T_s \omega_e(t)\zeta i_q(t)\left(\frac{\tilde{L}_q}{\tilde{L}_d} - \frac{L_q}{L_d}\right) \\ & + T_s \zeta u_d(t)\left(\frac{1}{\tilde{L}_d} - \frac{1}{L_d}\right) \end{aligned} \tag{21}$$

Through the above analysis, it can be seen that the actual value of the stator resistance can be decoupled from (21), resulting in

$$\tilde{R}_s = \frac{IR}{-\frac{T_s}{L_d}\zeta i_d(t)} \tag{22}$$

Substituting (16) and (22) into the mathematical expression (1) for permanent magnet synchronous motors decouples ψ_f, as shown in (23):

$$\tilde{\psi}_f = \frac{1}{\omega_e(t)}\left[u_q(t) - \tilde{L}_q\frac{di_q}{dt} - \tilde{L}_d\omega_e(t)i_d(t) - \tilde{R}_s i_q(t)\right] \tag{23}$$

In summary, (16), (22) and (23) are decoupling expressions for motor inductance, resistance, magnetic flux, and other parameters. By decoupling the parameters, the accuracy of parameter identification can be improved, and the control performance of the motor can also be improved.

It is important to note that while using the decoupling formula to decouple parameters, the denominator should not be zero. Therefore, at time t, it is detected that $||u_d(t) - u_d(t-1)| < 1$, $||u_q(t) - u_q(t-1)| < 1$, $\zeta i_d(t) < 0.01$, and $\omega_e(t) < 1$, where the motor parameter values are retained, the parameter estimates should be expressed as in (24).

$$\tilde{L}_d(t) = \tilde{L}_d(t-1), \tilde{L}_q(t) = \tilde{L}_q(t-1), \tilde{R}_s(t) = \tilde{R}_s(t-1), \tilde{\psi}_f(t) = \tilde{\psi}_f(t-1) \tag{24}$$

It should be noted that (21) uses voltage values rather than voltage differences, $u_q(t)$ should be subtracted from the voltage change value caused by nonlinear factors in the inverter.

4. Low-Complexity State Feedback Controller

4.1. Controller Design

The design of a time-delay tracking controller mainly includes the design of time performance functions and the establishment of error transfer functions. Selecting appropriate error transfer functions ensures the dynamic characteristics of the system during convergence.

Define the time performance function:

$$\rho = (\rho_0 - \varepsilon)e^{-\lambda t} + \varepsilon \tag{25}$$

where ρ_0 is the initial value of the time performance, which can affect the convergence speed of the error system, $\lambda > 0$, and ε affects the width of the error band. The error performance transfer function of the controller is designed as follows:

$$h_{i_d} = r_{i_d}\ln(1 - r_{i_d}^2) \tag{26}$$

where r_{id} is an intermediate variable defined as

$$\begin{cases} e_{i_d} = i_d - i_d^{ref} \\ r_{i_d} = e_{i_d}/\rho \end{cases} \tag{27}$$

where r_{id} and h_{id} are intermediate variables, i_d is the actual current of the d-axis during motor operation, and i_d^{ref} is the expected current calculated through the motor mathematical model.

From (27), it can be seen that when $|r_{id}| < 0$, $|e_{id}|$ satisfies $-\rho < |e_{id}| < \rho$; at this point, the d-axis current error will be within the envelope of the performance function.

Differentiating (26) yields

$$\begin{cases} \dot{h}_{i_d} = \lambda_{i_d} + \tau_{i_d} \frac{u_d - R_s i_d + p_n L_s \omega_m i_q}{L_s} \\ \lambda_{i_d} = \left\{ r_{i_d} \dot{\rho} \left[-\ln(1 - r_{i_d}^2) + \frac{-2r_{i_d}^2}{1 - r_{i_d}^2} \right] \right\} / \rho \\ \tau_{i_d} = \left[-\ln(1 - r_{i_d}^2) + \frac{-2r_{i_d}^2}{1 - r_{i_d}^2} \right] / \rho \end{cases} \tag{28}$$

where λ_{id} and h_{id} are summary functions, and their signs are always opposite.

Define the electrical parameter estimation error as in (29):

$$\begin{cases} e_R = R_s - \hat{R}_s \\ e_{L_s} = L_s - \hat{L}_s \\ e_{\psi_f} = \psi_f - \hat{\psi}_f \end{cases} \tag{29}$$

From (29), we can obtain the derivatives of the estimation errors of each electrical parameter as follows:

$$\begin{cases} \dot{e}_R = -\dot{\hat{R}}_s \\ \dot{e}_{L_s} = -\dot{\hat{L}}_s \\ \dot{e}_{\psi_f} = -\dot{\hat{\psi}}_f \end{cases} \tag{30}$$

Enter the values of each function in the above model into the controller, ignore the maximum overshoot, and use a symmetric performance function to constrain the update rate of the output tracking error. The resulting controller performance curve is shown in Figure 2:

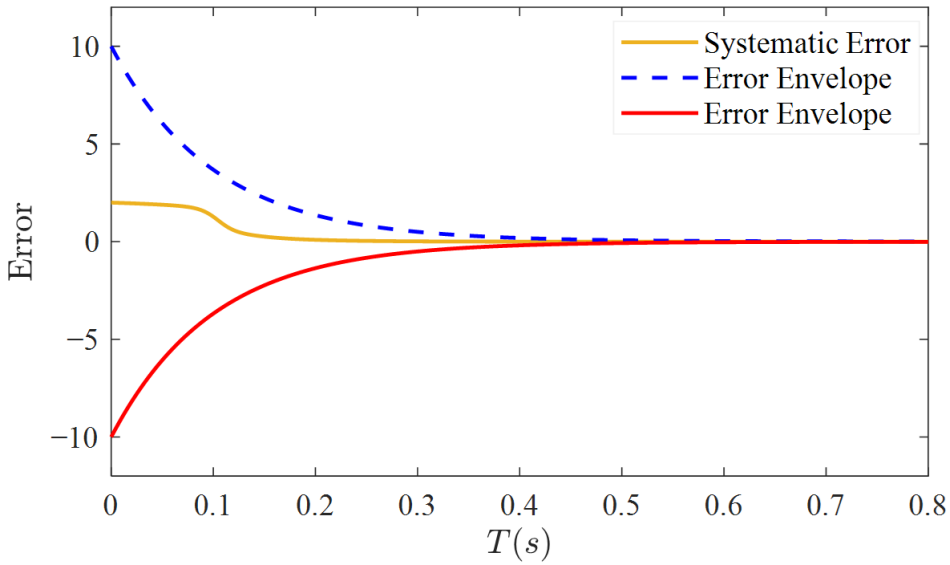

Figure 2. Controller performance curve.

When the trajectory of the error system approaches the error band, the convergence speed will significantly decrease and gradually converge to 0. When the system's convergence state shows a tendency to deviate from the error band, the performance function forces the error function to remain within the error band and alters its convergence law. This new convergence law can shorten the time required for the error system to reach the error band and effectively attenuate the oscillation phenomenon caused by the rapid change in the convergence law when reaching the critical state.

4.2. Stability Proof of Resistance and Inductance Parameter Identification Based on LCSPC

Select the Lyapunov function $V = s^2/2$ to verify the stability of the proposed controller when the following conditions are satisfied:

$$\dot{V} = s\dot{s} \leq 0 \tag{31}$$

Therefore, define the Lyapunov function V_1 as

$$V_1 = \frac{L_s h_{i_d}^2 + e_R^2 + e_{L_s}^2}{2} \tag{32}$$

Differentiating (32) yields

$$\begin{aligned} \dot{V}_1 &= L_s h_{i_d} h_{i_d} + e_R \dot{e}_R + e_{L_s} \dot{e}_{L_s} \\ &= \left[\lambda_{i_d} + \tau_{i_d} h_{i_d} \left(u_d - R_s i_d + L_s p_n \omega_m i_q\right)\right] - e_{R_s} \dot{e}_{R_s} - e_{L_s} \dot{e}_{L_s} \end{aligned} \tag{33}$$

The control rate of u_d is designed as $u_d = u_{d0} + u_{d1}$, where u_{d0} is the error term and u_{d1} is the compensation term, expressed as follows:

$$\begin{cases} u_{d0} = \hat{R} i_d - \hat{L}_s p_n \omega_m i_q \\ u_{d1} = -h_{id} \tau_{id} - k_1 r_{id} \end{cases} \tag{34}$$

Substituting u_d into (33), we can simplify it to

$$\begin{aligned} V_1 &= L_s h_{id} \lambda_{id} + h_{id} \tau_{id} \left[\left(\hat{R}_s - R_s\right) i_d + \left(L_s - \hat{L}_s\right) P_n \omega_m i_q - h_{id} \tau_{id} - k_1 r_{id}\right] - e_{R_s} \dot{e}_{R_s} - e_{L_s} \dot{e}_{L_s} \\ &= L_s h_{id} \lambda_{td} + \left\{h_{id} \tau_{id} \left[\left(-e_{R_s} i_d\right) + e_{L_s} P_n \omega_m i_q\right] - e_{R_s} \hat{R}_s - e_{L_s} \hat{L_s}\right\} - h_{i_d}^2 \tau_{i_d}^2 - k_1 h_{id} \tau_{id} r_{i_d} \end{aligned} \tag{35}$$

From (35), we can obtain the adaptive update rates for $\dot{\hat{R}}_s$ and $\dot{\hat{L}}_s$:

$$\begin{cases} \dot{\hat{R}}_s = -h_{id} \tau_{id} i_d + k_R e_R \\ \dot{\hat{L}}_s = h_{id} \tau_{id} P_n \omega_m i_q + k_{L_s} e_{L_s} \end{cases} \tag{36}$$

The expression for $\dot{V}$ can be updated to

$$\dot{V}_1 = L_s h_{id} \lambda_{id} - h_{i_d}^2 \tau_{i_d}^2 - k_1 h_{id} \tau_{id} r_{i_d} - k_R e_R^2 - k_{L_s} e_{L_s}^2 \tag{37}$$

At this point, $\dot{V}_1 \leq 0$ is satisfied, and the system meets the stability conditions.

4.3. Proof of Stability of Magnetic Flux Parameter Identification

From the mathematical model of the motor, it can be seen that analyzing the cross-axis current yields the magnetic flux parameter identification expression. The control rate of u_q is designed as

$$\begin{cases} u_q = u_{q0} + u_{q1} \\ u_{q0} = \hat{R}_s i_q + \hat{L}_s p_n \omega_m i_d + \hat{\psi}_f p_n \omega_m \\ u_{q1} = -h_{iq} \tau_{iq} - k_2 r_{iq} \end{cases} \tag{38}$$

Define the Lyapunov function at this point as

$$V_2 = \frac{L_s h_{i_q}^2 + e_{L_s}^2 + e_{\psi_f}^2}{2} \tag{39}$$

V_2 can be simplified to

$$\dot{V}_2 = L_s h_{i_q} \lambda_{i_q} + h_{i_q} \tau_{i_q} \left(u_q - R_s i_q - L_s p_n \omega_m i_d - \psi_f p_n \omega_m \right) - e_{L_s} \dot{\hat{L}}_s - e_{\psi_f} \dot{\hat{\psi}}_f \tag{40}$$

Substituting (38) into (40) yields

$$V_2 = L_s h_{i_q} \lambda_{i_q} + \left[h_{i_q} \tau_{i_q} \left(-e_{R_z} i_q - e_{L_z} p_n \omega_m i_d - e_{\psi_f} p_n \omega_m \right) - e_{L_z} \dot{\hat{L}}_s - e_{\psi_f} \dot{\hat{\psi}}_f \right] - h_{i_q}^2 \tau_{i_q}^2 - k_2 h_{i_q} \tau_{i_q} r_{i_q} \tag{41}$$

From (41), the expression for $\dot{\hat{\psi}}_f$ is obtained as

$$\begin{cases} \dot{\hat{L}}_s = -h_{i_q} \tau_{i_q} p_n \omega_m i_d + k_{i_d} e_{i_d} \\ \dot{\hat{\psi}}_f = -h_{i_q} \tau_{i_q} p_n \omega_m + k_{\psi_f} e_{\psi_f} \end{cases} \tag{42}$$

The expression for $\dot{V}_2$ is updated to

$$V_2 = L_s h_{i_q} \lambda_{i_q} - h_{i_q}^2 \tau_{i_q}^2 - k_2 h_{i_q} \tau_{i_q} r_{i_q} - k_{i_q} e_{i_q}^2 - k_{\psi_f} e_{\psi_f}^2 - h_{i_q} \tau_{i_q} e_{R_s} i_q \tag{43}$$

At this point, $\dot{V}_2$ always satisfies the condition of being less than or equal to 0, meeting the stability requirement.

5. Simulation Analysis and Experimental Verification

To validate the identification accuracy of the LCSPC-DPCC, this paper establishes two different electrical parameter identification models for surface-mounted permanent magnet synchronous motors in Simulink: a novel deadbeat predictive current prediction control model based on the model reference adaptive identification algorithm and a deadbeat predictive current prediction control model based on low-complexity specified performance tracking. The motor parameters were identified in terms of identification accuracy, convergence speed, and load transients, further validating the advantages of LCSPC-DPCC over MRAS-DPCC.

5.1. Simulation Analysis

The parameters of the permanent magnet synchronous motor are shown in Table 1. During the simulation process, in order to more intuitively demonstrate the differences between the two identification algorithms, the rotor position information of both simulation models was fed back using an encoder. The simulation time of the system was fixed at 3 s, and the fixed step size was set to 1 µs.

Table 1. Experimental platform parameters.

Items	Value	Parameters	Value
Rated speed	3000 RPM	Stator resistance R_s	$0.56 \pm 10\%$ Ω
Rated power	64 W	Stator inductance L_s	$0.62 \pm 20\%$ mH
Rated current	4 A	Flux linkage ψ_f	0.0083 Wb
Rated toque	0.2 N·m	Rotational inertia J	1.5 kg·cm^2
Pole pairs p_n	4	ρ_{0°	6
ε	0.005	λ	10

To ensure the reliable operation of the parameter feedback module and the control accuracy of the motor control system, constant-speed no-load (1000 r/min, 2000 r/min, 3000 r/min) and variable-speed no-load simulations of the algorithm were first conducted. The variable-speed control simulation refers to an initial speed of 1000 r/min, reaching 2000 rpm at 1 s, and reaching the rated speed of 3000 rpm at 2 s.

Figures 3 and 4 show the deviation between the actual current and the reference current when the motor is running at a constant speed and at a variable speed under no-load conditions. Figure 5 shows the electrical parameter identification results obtained using LCSPC-DPCC and MRAS-DPCC when the motor is running under no-load conditions.

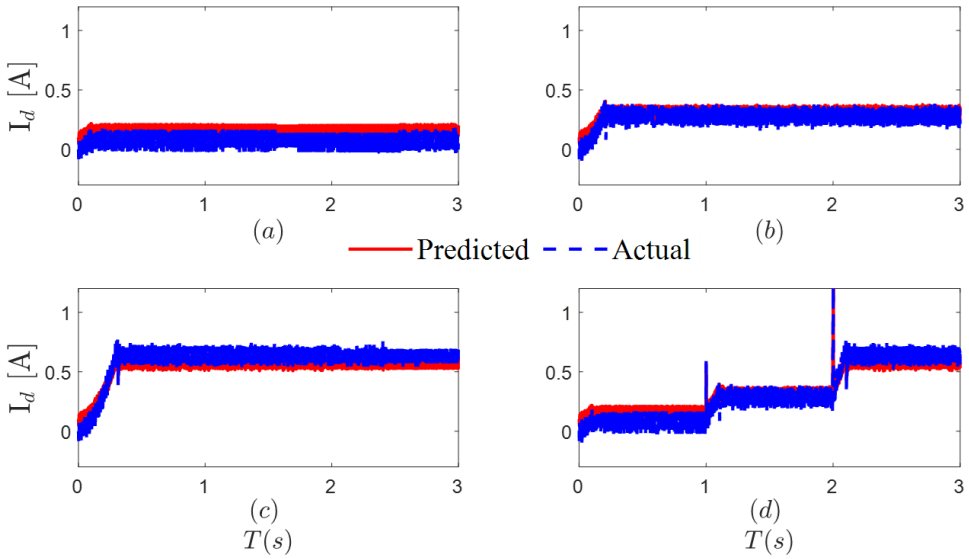

Figure 3. Actual and estimated values of d-axis current at different expected speeds. (**a**) 1000 r/min. (**b**) 2000 r/min. (**c**) 3000 r/min. (**d**) Variable speed.

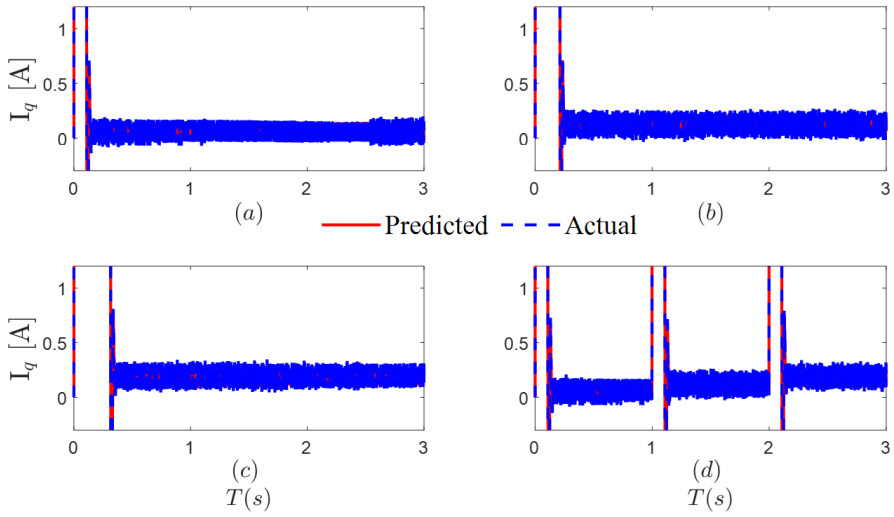

Figure 4. Actual and estimated values of q-axis current at different expected speeds. (**a**) 1000 r/min. (**b**) 2000 r/min. (**c**) 3000 r/min. (**d**) Variable speed.

As shown in Figure 5, both algorithms can effectively track the actual current. However, since MRAS-DPCC uses the real-time feedback of the *d-q* axis actual current from the motor and the motor mathematical model for parameter identification, this inevitably leads to the impact of parameter mismatch on the output torque. Additionally, due to varying degrees of current deviation, the results of parameter identification will also have a certain degree of error. In contrast, the LCSPC-DPCC uses the motor mathematical model after decoupling compensation for parameter identification, effectively reducing the impact of current disturbances on the accuracy of parameter identification.

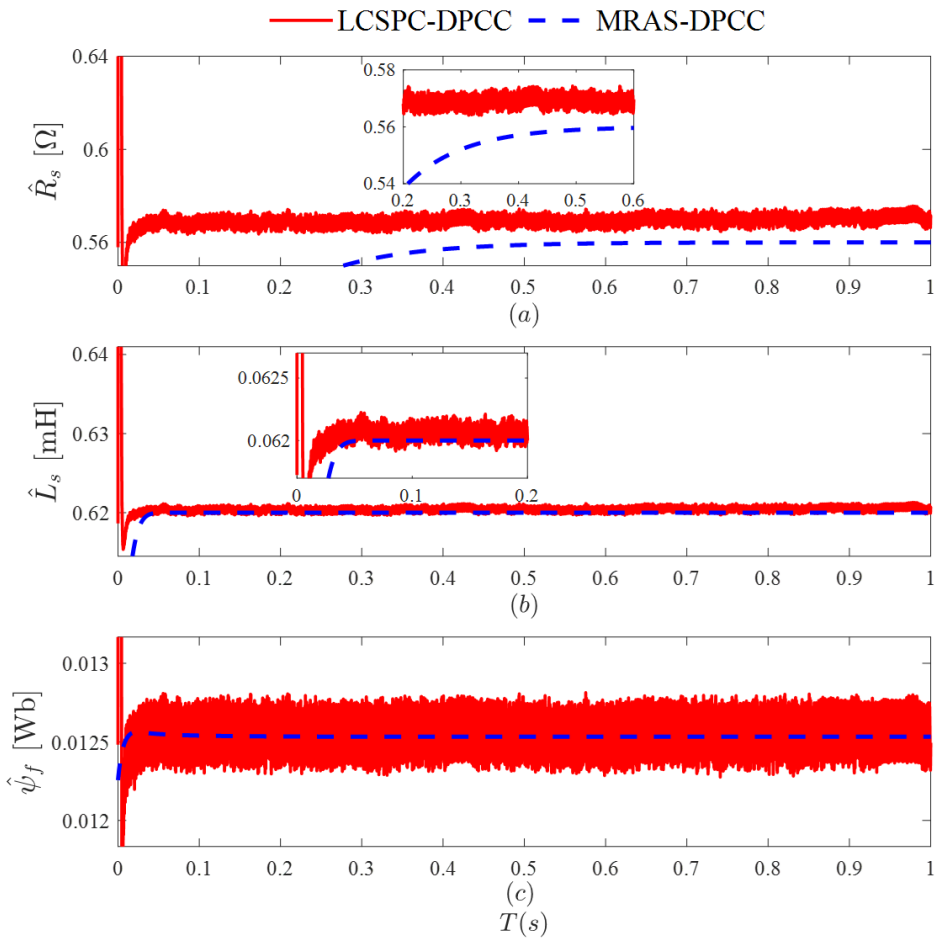

Figure 5. Identification results of various parameters at different expected speeds. (**a**) 1000 r/min. (**b**) 2000 r/min. (**c**) 3000 r/min.

To study the dynamic performance of the control system under the two algorithms, a load test was conducted. A sudden load of 0.2 Nm was applied at 0.5 s, followed by another sudden increase of 0.2 Nm at 1.5 s, and then all loads were cleared at 2.5 s. Algorithm simulations were performed for the above scenario to obtain the predicted and actual currents in the d-q axes, with the results shown in Figure 6. Additionally, the LCSPC-DPCC and MRAS-DPCC algorithms were used to compare the identification of motor electrical parameters, with the results shown in Figure 7.

Figure 6 shows the temporary mismatch of Ls caused by load changes, which in turn leads to fluctuations in the d/q-axis currents. When the load changes, the d-q-axis currents oscillate within a certain range as the estimated value of Ls changes. Once Ls identification is complete, the d-q-axis currents gradually stabilize. Since *d-q* axis currents exhibit oscillation issues, using MRAS for parameter identification also introduces oscillations into the identification results. This causes the MRAS algorithm's identification results to oscillate around the actual values, leading to continuous fluctuations in the electrical parameter feedback results and ultimately reducing the motor's control accuracy. The LCSPC-DPCC algorithm designed in this paper decouples and compensates for resistance, inductance, and magnetic flux from the perspective of the motor's mathematical model. Therefore, the identification results obtained using this algorithm have higher accuracy and can overcome the influence of external disturbances on the algorithm, consistently meeting the high-precision parameter feedback requirements of the motor control system.

As shown by the simulation results, the accuracy of the resistance, inductance, and magnetic flux identified using MRAS-DPCC is 0.5%, 1.9%, and 1.84%, respectively,

while the identification accuracies of the various parameters using LCSPC-DPCC are 0.26%, 0.07%, and 0.24%, respectively, representing improvements of 48.1%, 96.2%, and 86.7% compared to MRAS-DPCC.

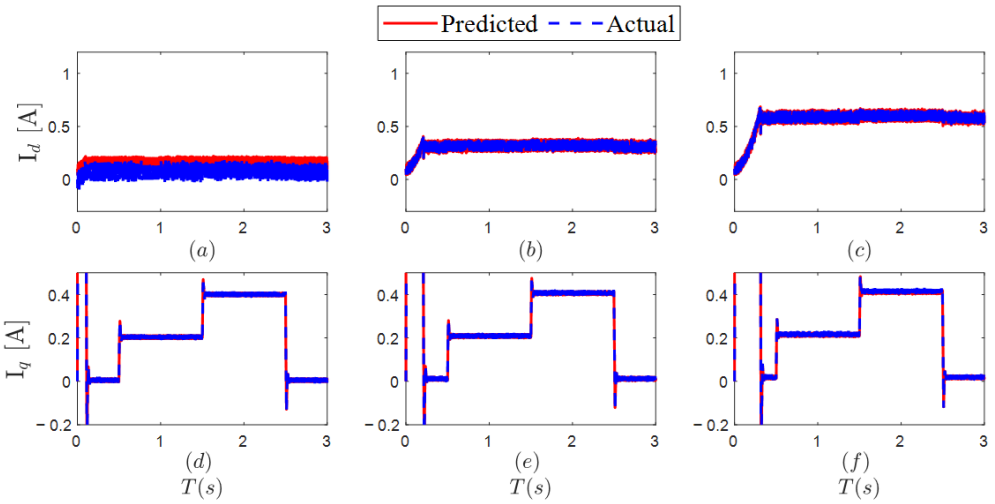

Figure 6. Actual and estimated values of d/q-axis currents at different expected speeds under load conditions. (**a**) d-axis currents-1000 r/min. (**b**) d-axis currents-2000 r/min. (**c**) d-axis currents-3000 r/min. (**d**) q-axis currents-1000 r/min. (**e**) q-axis currents-2000 r/min. (**f**) q-axis currents-3000 r/min.

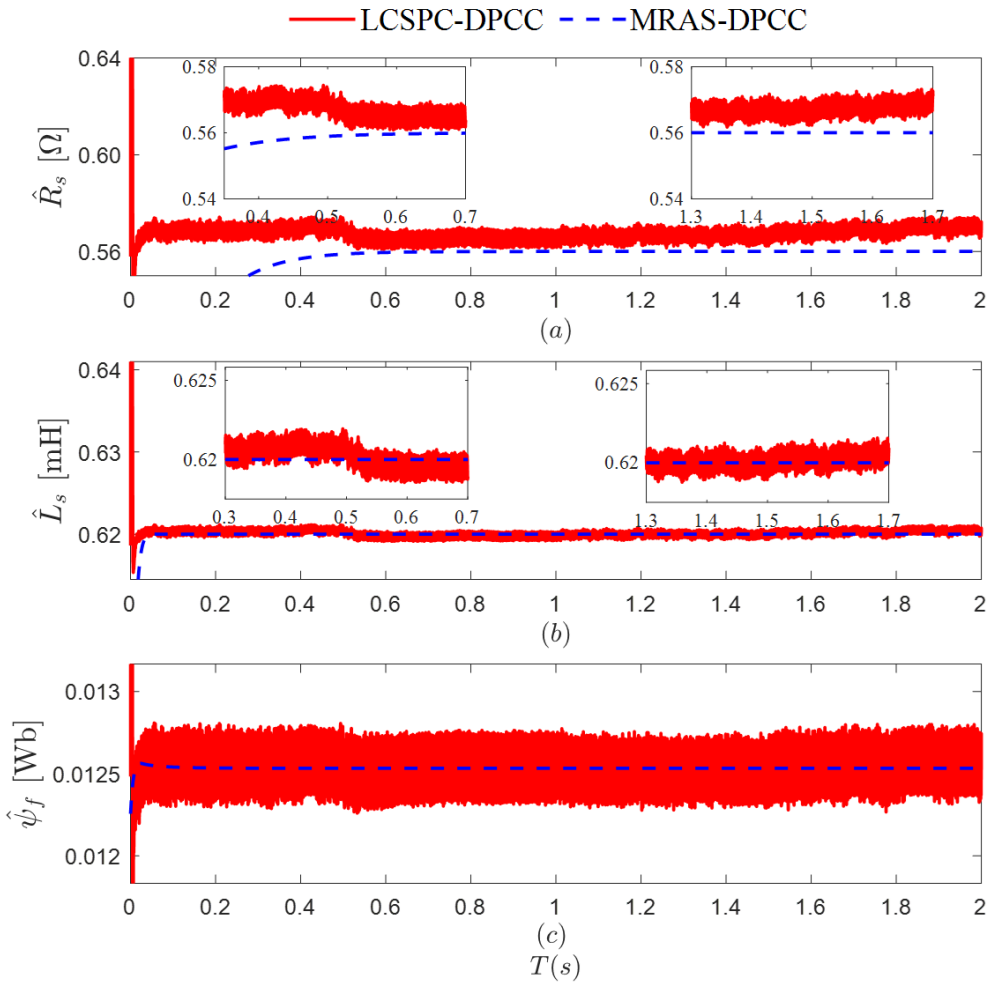

Figure 7. Identification results of various parameters under different expected speeds under load conditions. (**a**) 1000 r/min. (**b**) 2000 r/min. (**c**) 3000 r/min.

5.2. Experimental Verification

To further test the performance of LCSPC-DPCC, a permanent magnet synchronous motor control system experimental platform was constructed as shown in Figure 8. Due to the low-complexity advantage of the algorithm, the STM32F407 microcontroller was used to implement the control algorithm.

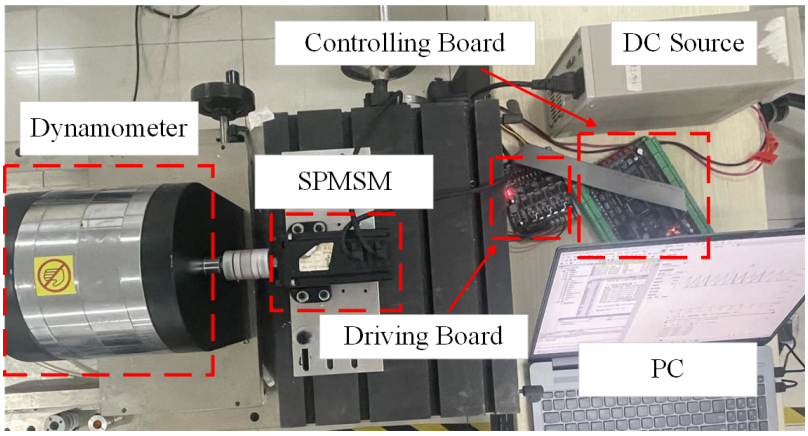

Figure 8. Experimental platform of permanent magnet synchronous motor control system.

(1) No-load test: Figure 9 shows the d/q-axis current waveforms corresponding to different speeds under no-load conditions. The expected speeds during the test were set to 1000 r/min, 2000 r/min, 3000 r/min, and variable speed.

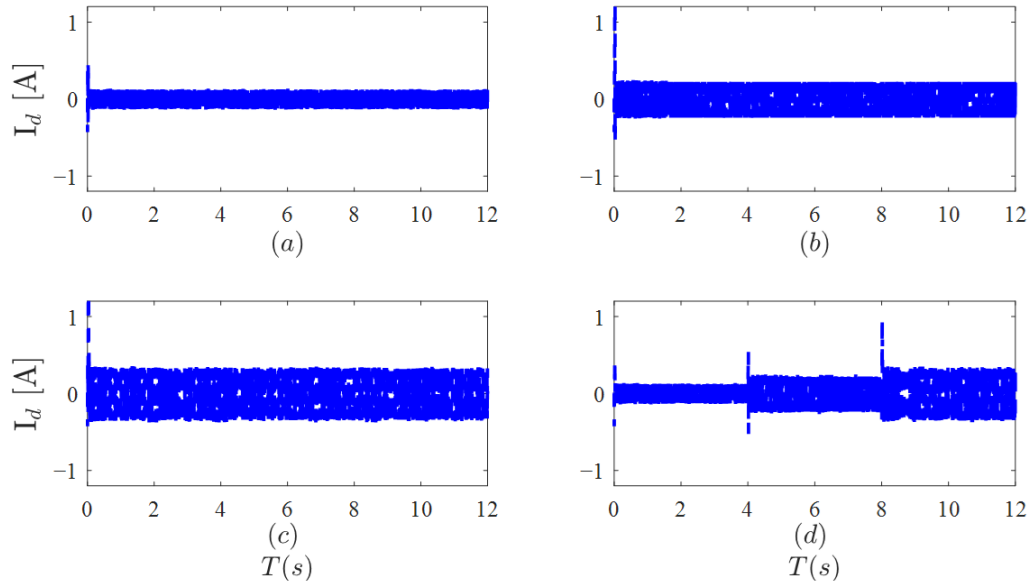

Figure 9. d-axis current waveforms at different expected speeds. (**a**) 1000 r/min. (**b**) 2000 r/min. (**c**) 3000 r/min. (**d**) Variable speed.

To verify the feasibility of zero-beat current predictive control during motor operation, an incremental encoder was used for rotor information feedback. As shown in Figures 9 and 10, the non-steady-state errors caused by the motor's own mechanical characteristics result in the *d-q* axis currents fluctuating around the desired values under different operating speeds. When the speed is switched to 2000 r/min at 4 s, the *d-q* axis currents exhibit a significant fluctuation lasting approximately 0.2 s. When the speed is switched to 3000 r/min at 8 s, the fluctuations in the *d-q* axis currents become even more pronounced.

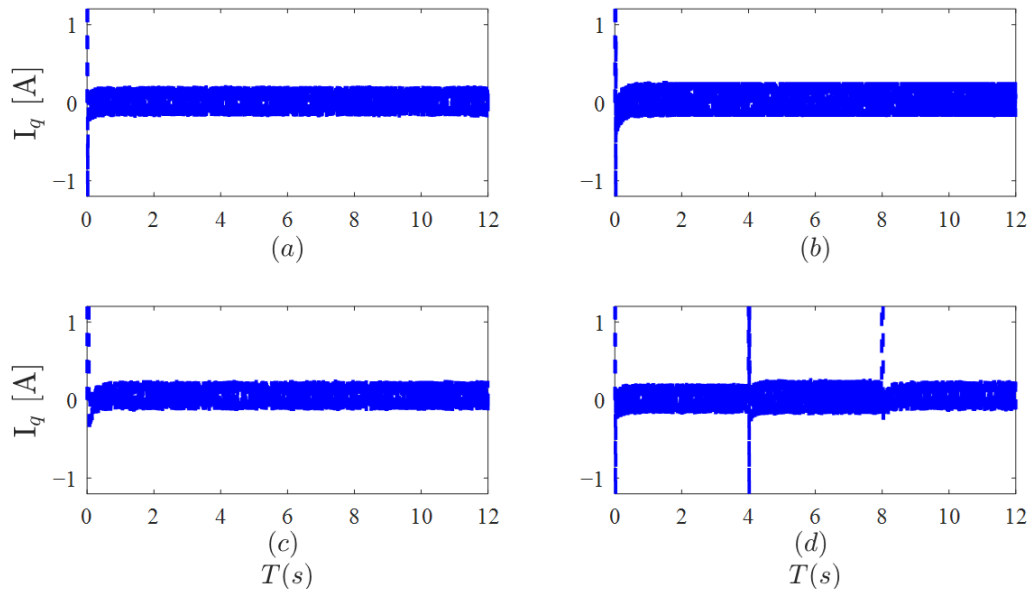

Figure 10. q-axis current waveforms at different expected speeds. (**a**) 1000 r/min. (**b**) 2000 r/min. (**c**) 3000 r/min. (**d**) Variable speed.

As shown in Figure 11, during the speed-up phase, the motor current is in a fluctuating state and cannot provide stable and reliable algorithm inputs. Therefore, the identification results of various parameters during the speed-up phase exhibit significant deviations from actual values. The convergence times for the parameters R_s, L_s, and ψ_f are 4.2 s, 4.5 s, and 4.5 s, respectively. From the perspective of algorithm input: Once the actual speed reaches the desired speed, the *d-q* axis current of the motor becomes relatively stable, leading to a stable input for the LCSPC. This, in turn, causes the parameter identification values output by the LCSPC to stabilize. From the perspective of algorithm advantages, since the *d-q* axis current is a critical factor influencing the decoupling model of the motor in this paper, ensuring the stability of the *d-q* axis current is of utmost importance. In utilizing DPCC, the *d-q* axis current is consistently maintained within a certain amplitude range. Therefore, LCSPC and DPCC can complement each other to achieve high-precision parameter identification of the motor.

(2) Load variation test: Verify the *d-q* axis current of the motor under conditions such as sudden increase/decrease, observe the effect of the load on the current, and verify the reliability of the algorithm.

As shown in Figure 12, when sudden loading/unloading occurs at 8 s, 16 s, and 24 s, Id remains within a certain range throughout the process and does not change with sudden loading/unloading; however, Iq changes proportionally with the load. The *d-q* axis current is a core parameter for motor electrical parameter identification, so ensuring high-precision, low-latency feedback of the *d-q* axis current is the core of the entire identification system. DPCC has high-precision current tracking capabilities, so the difference between the actual *d-q* axis current and the expected current is small, thereby ensuring high-precision feedback of the *d-q* axis current.

As shown in Figure 13, before the actual speed reaches the desired speed, due to fluctuations in the *d-q* axis current, the identification values of R_s, L_s, and ψ_f exhibit significant errors, which persist until identification is completed around 8 s. However, after adding a 0.2 N·m load at 8 s, the *d-q* axis current experiences short-term feedback fluctuations, resulting in increased identification errors for all parameters, which stabilize after approximately 0.3 s. When an additional 0.2 N·m load is applied at 16 s, the fluctuations in the *d-q* currents cause the identification results of the parameters to exhibit overshoot for approximately

0.2 s, after which they stabilize. Finally, after the load is suddenly reduced to zero at 24 s, the identification results of the parameters fluctuate for 0.5 s before stabilizing.

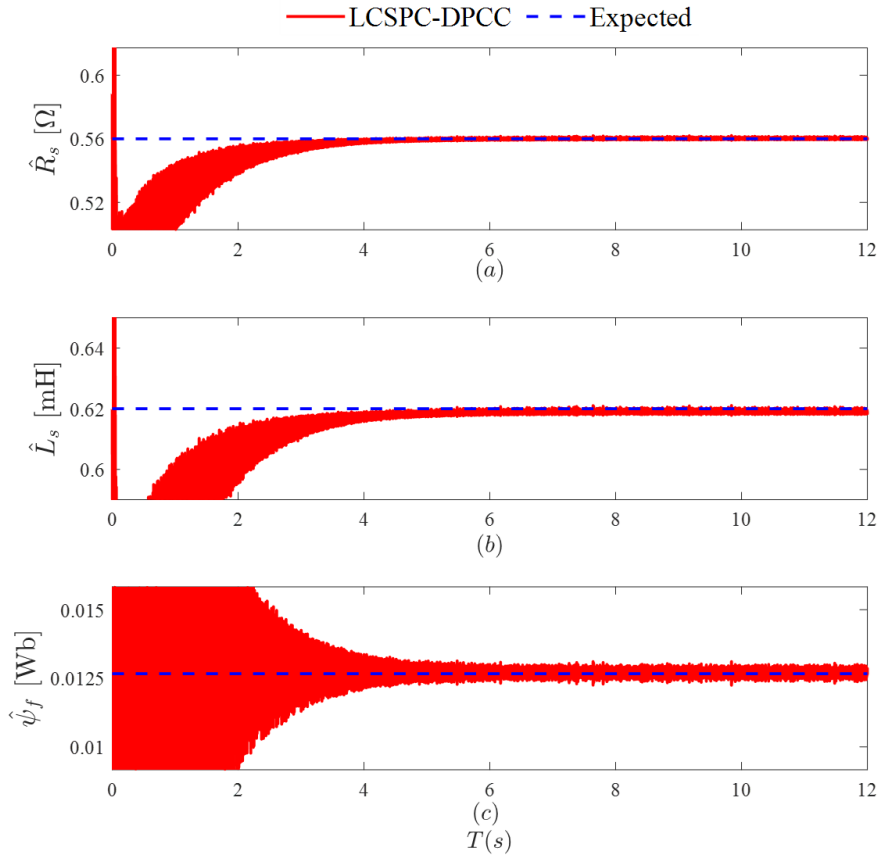

Figure 11. Motor parameter identification results. (**a**) Identification results of R_s. (**b**) Identification results of L_s. (**c**) Identification results of ψ_f.

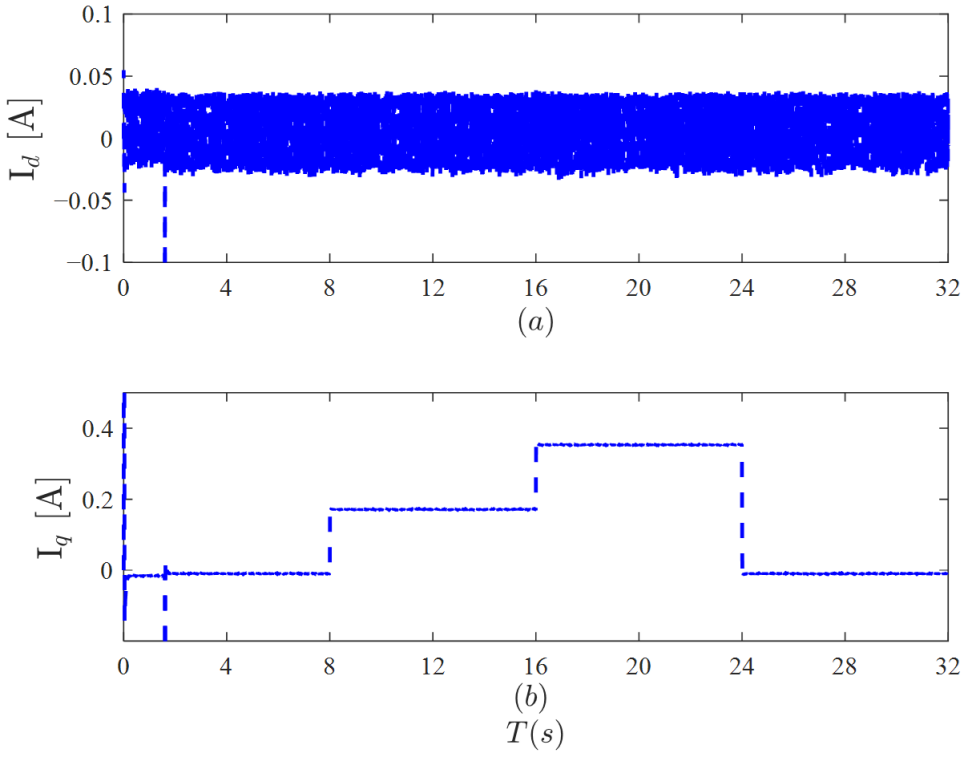

Figure 12. Actual *d*-*q* current under variable load. (**a**) d-axis current. (**b**) q-axis current.

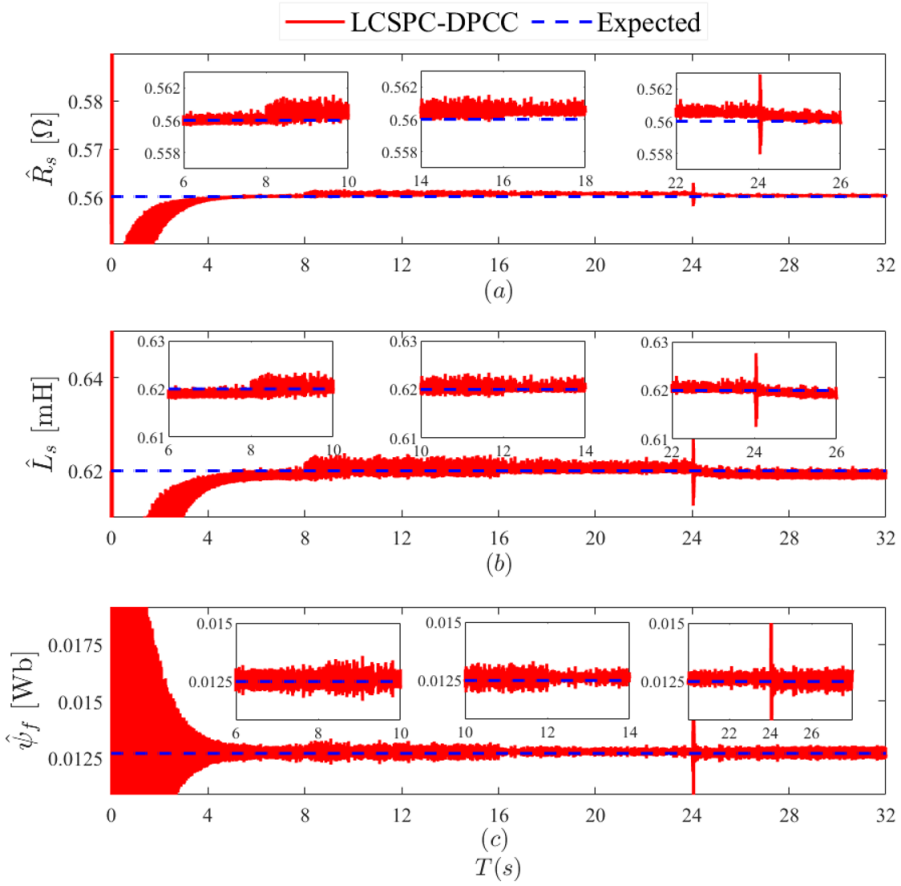

Figure 13. Identification results of parameters to be identified under variable load conditions. (**a**) Identification results of R_s. (**b**) Identification results of L_s. (**c**) Identification results of ψ_f.

6. Conclusions

To address the decline in control accuracy caused by parameter mismatch in joint-driven permanent magnet synchronous motor drive systems and enhance the control system's disturbance rejection capability, an enhanced DPCC multi-parameter discrete system identification scheme based on LCSPC is proposed. The research findings are summarized as follows:

(1) Deriving a transient current error model from the motor model solves the problem of matrix rank deficiency during multi-parameter identification. It also reduces the loss of identification accuracy caused by parameter coupling.

(2) A control algorithm for an LCSPC was designed based on a discrete mathematical model of the motor. This algorithm has low model complexity and automatically feeds identification results back into the control system. It imposes minimal computational demands on the controller, thereby meeting cost requirements within the intelligent manufacturing sector.

(3) Both simulation analysis and experimental results demonstrate that the proposed control algorithm not only satisfies the identification requirements of low electrical parameter error and rapid convergence but also treats external disturbances as controller convergence curves during different motor operating states. Adjusting the parameters achieves high-precision motor control.

(4) Although the presented algorithm shows great potential for practical application, there are still some challenges in the control process, such as deadband output voltage compensation and DPCC accuracy.

Author Contributions: Conceptualization, Z.T. and Y.Z.; methodology, M.L.; software, M.L.; validation, Y.Z., Z.T. and H.Y.; formal analysis, L.W.; investigation, Y.Z.; resources, Y.Z.; data curation, L.W.; writing—original draft preparation, Y.Z.; writing—review and editing, Y.Z.; visualization, Z.T.; supervision, Z.T.; project administration, Y.Z.; funding acquisition, Y.Z. All authors have read and agreed to the published version of the manuscript.

Funding: This research was funded by the National Natural Science Foundation of China, 52477095.

Data Availability Statement: The original contributions presented in this study are included in the article. Further inquiries can be directed to the corresponding author.

Conflicts of Interest: The authors declare no conflicts of interest.

References

1. Xiang, Z.; Wei, J.; Zhu, X. Torque ripple suppression of a PM vernier machine from perspective of time and space harmonic magnetic field. *IEEE Trans. Ind. Electron.* **2023**, *71*, 10150–10161. [CrossRef]
2. Luan, M.; Ruan, J.; Zhang, Y.; Yan, H.; Wang, L. An improved adaptive Finite-Time Super-Twisting sliding mode observer for the sensorless control of permanent magnet synchronous motors. *Actuators* **2024**, *13*, 395. [CrossRef]
3. Xiang, Z.; Zhou, Y.; Zhu, X.; Quan, L.; Fan, D.; Liu, Q. Research on characteristic airgap harmonics of a double-rotor flux-modulated PM motor based on harmonic dimensionality reduction. *IEEE Trans. Transp. Electrif.* **2023**, *10*, 5750–5761. [CrossRef]
4. Jain, H.; Babel, P. A comprehensive survey of PID and pure pursuit control algorithms for autonomous vehicle navigation. *arXiv* **2024**, arXiv:2409.09848. [CrossRef]
5. Shawier, A.; Abdel-Azim, W.E.; Yepes, A.G.; Abdel-Khalik, A.S.; Hamad, M.S.; Ahmed, S.; Doval-Gandoy, J. Hysteresis current control for six-phase induction motor drives with reduced ripple and improved tracking based on subspace decomposition and restrained voltage vectors. *IEEE Trans. Ind. Electron.* **2023**, *71*, 6534–6545. [CrossRef]
6. Peng, J.; Yao, M. Overview of predictive control technology for permanent magnet synchronous motor systems. *Appl. Sci.* **2023**, *13*, 6255. [CrossRef]
7. Zhang, Y.; Xia, B.; Yang, H.; Rodriguez, J. Overview of model predictive control for induction motor drives. *Chin. J. Electr. Eng.* **2016**, *2*, 62–76. [CrossRef]
8. Brosch, A.; Wallscheid, O.; Böcker, J. Time-optimal model predictive control of permanent magnet synchronous motors considering current and torque constraints. *IEEE Trans. Power Electron.* **2023**, *38*, 7945–7957. [CrossRef]
9. Li, T.; Sun, X.; Lei, G.; Guo, Y.; Yang, Z.; Zhu, J. Finite-control-set model predictive control of permanent magnet synchronous motor drive systems—An overview. *IEEE/CAA J. Autom. Sin.* **2022**, *9*, 2087–2105. [CrossRef]
10. Ismail, M.M.; Xu, W.; Ge, J.; Tang, Y.; Junejo, A.K.; Hussien, M.G. Adaptive linear predictive model of an improved predictive control of permanent magnet synchronous motor over different speed regions. *IEEE Trans. Power Electron.* **2022**, *37*, 15338–15355. [CrossRef]
11. Niu, L.; Yang, M.; Xu, D.g. Deadbeat predictive current control for PMSM. In Proceedings of the 2012 15th International Power Electronics and Motion Control Conference (EPE/PEMC), Novi Sad, Serbia, 4–6 September 2012; IEEE: New York, NY, USA, 2012; p. LS6b-1.
12. Wang, Y.; Liao, W.; Huang, S.; Zhang, J.; Yang, M.; Li, C.; Huang, S. A robust DPCC for IPMSM based on a full parameter identification method. *IEEE Trans. Ind. Electron.* **2022**, *70*, 7695–7705. [CrossRef]
13. Zhang, S.; Shen, A.; Luo, X.; Tang, Q.; Li, Z. An adaptive strategy for PMSM-based disturbance estimation and online parameter identification. *IEEE/ASME Trans. Mechatron.* **2023**, *29*, 2522–2533. [CrossRef]
14. Luan, M.; Zhang, Y.; Ruan, J.; Guo, Y.; Wang, L.; Min, H. Research on the Mechanical Parameter Identification and Controller Performance of Permanent Magnet Motors Based on Sensorless Control. *Actuators* **2024**, *13*, 525. [CrossRef]
15. Chen, Y.; Chen, D.; Li, Z.; Lei, H.; Zhu, H. Off-line Parameter Identification of Permanent Magnet Synchronous Motor. *J. Physics Conf. Ser. IOP Publ.* **2021**, *2076*, 012096. [CrossRef]
16. Morimoto, S.; Sanada, M.; Takeda, Y. Mechanical sensorless drives of IPMSM with online parameter identification. *IEEE Trans. Ind. Appl.* **2006**, *42*, 1241–1248. [CrossRef]
17. Li, X.; Kennel, R. General formulation of Kalman-filter-based online parameter identification methods for VSI-fed PMSM. *IEEE Trans. Ind. Electron.* **2020**, *68*, 2856–2864. [CrossRef]
18. Brosch, A.; Wallscheid, O.; Böcker, J. Long-term memory recursive least squares online identification of highly utilized permanent magnet synchronous motors for finite-control-set model predictive control. *IEEE Trans. Power Electron.* **2022**, *38*, 1451–1467. [CrossRef]

19. Qi, X.; Sheng, C.; Guo, Y.; Su, T.; Wang, H. Parameter identification of a permanent magnet synchronous motor based on the model reference adaptive system with improved active disturbance rejection control adaptive law. *Appl. Sci.* **2023**, *13*, 12076. [CrossRef]
20. Yao, X.; Huang, S.; Wang, J.; Ma, H.; Zhang, G.; Wang, Y. Improved ROGI-FLL-based sensorless model predictive current control with MRAS parameter identification for SPMSM drives. *IEEE J. Emerg. Sel. Top. Power Electron.* **2022**, *11*, 1684–1695. [CrossRef]
21. Rashed, M.; MacConnell, P.F.; Stronach, A.F.; Acarnley, P. Sensorless indirect-rotor-field-orientation speed control of a permanent-magnet synchronous motor with stator-resistance estimation. *IEEE Trans. Ind. Electron.* **2007**, *54*, 1664–1675. [CrossRef]
22. Wu, K.; Lin, Y. Sensorless speed control of PMLSM via adaptive interconnected state observer. *Int. J. Control. Autom. Syst.* **2022**, *20*, 3822–3831. [CrossRef]
23. Colombo, L.; Corradini, M.L.; Cristofaro, A.; Ippoliti, G.; Orlando, G. An embedded strategy for online identification of PMSM parameters and sensorless control. *IEEE Trans. Control Syst. Technol.* **2018**, *27*, 2444–2452. [CrossRef]
24. Reddy, G.B.; Poddar, G.; Muni, B.P. Parameter estimation and online adaptation of rotor time constant for induction motor drive. *IEEE Trans. Ind. Appl.* **2022**, *58*, 1416–1428. [CrossRef]
25. Wang, L.; Zhang, S.; Zhang, C.; Zhou, Y. An improved deadbeat predictive current control based on parameter identification for PMSM. *IEEE Trans. Transp. Electrif.* **2023**, *10*, 2740–2753. [CrossRef]

Disclaimer/Publisher's Note: The statements, opinions and data contained in all publications are solely those of the individual author(s) and contributor(s) and not of MDPI and/or the editor(s). MDPI and/or the editor(s) disclaim responsibility for any injury to people or property resulting from any ideas, methods, instructions or products referred to in the content.